Synthesis of novel mesoporous selenium-doped biochar with high-performance sodium diclofenac and reactive orange 16 dye removals

Glaydson S. dos Reis [a,*], Julie Thivet [a,b], Ewen Laisné [a,c], Varsha Srivastava [d], Alejandro Grimm [a], Eder C. Lima [e,f], Davide Bergna [d], Tao Hu [d], Mu. Naushad [f], Ulla Lassi [d]

[a] Department of Forest Biomaterials and Technology, Biomass Technology Centre, Swedish University of Agricultural Sciences, Umeå SE-901 83, Sweden
[b] Ecole Nationale Supérieure de Chimie de Montpellier, Montpellier, France
[c] IMT Mines Albi-Carmaux, 81000 Albi, France
[d] Research Unit of Sustainable Chemistry, Faculty of Technology, University of Oulu, FI-90014 Oulu, Finland
[e] Institute of Chemistry, Federal University of Rio Grande do Sul (UFRGS), Porto Alegre, RS, Brazil
[f] Department of Chemistry, College of Science, King Saud University, P.O. Box 2455, Riyadh 11451, Saudi Arabia

ABSTRACT

In this study, for the first time, a selenium-doped mesoporous biochar was prepared and efficiently employed for sodium diclofenac and reactive orange 16 dye adsorption. The characterization results indicated that selenium doping had a remarkable impact on Biochar-Se morphological and physicochemical structures. The efficacy of developed biochar samples on reactive orange 16 (RO-16) and diclofenac (DCF) removals was fully investigated. For both molecules (DCF and RO-16), Liu's equilibrium model offered the best fitness with maximum adsorption capacity values of 355 mg g^{-1} for DCF and 538 mg g^{-1} for RO-16 for Biochar-Se. Multiple mechanisms including pore filling, π-π interaction, and hydrogen bonding between the Biochar-Se and DCF/RO-16 molecules were involved in the adsorption process. Se-nanoparticles formed metal–oxygen bonds, which boosted the adsorption of DCF and RO-16 molecules. The current work offered a feasible approach for the development of Se-doped biochar adsorbent that is incredibly effective in treating wastewater.

1. Introduction

Water contamination has been a serious problem worldwide for a long time, and anthropogenic activities related to pharmaceutical and textile industries have worsen the problem due to the release of colourful and drug-loaded effluents into waterbodies. It is reported that over 20% of the contamination of water worldwide is attributed to dyes and drugs (Abadi et al., 2023; Omorogie et al., 2021). Into the environment, these contaminants may cause damage to aquatic ecosystems as well as pose risks to human health (Farré et al., 2008; Lin et al., 2022). Thus, is mandatory to remove these contaminants from the effluents before they are discharged into natural waterbodies.

Several methodologies have been employed to treat effluents loaded with drugs and dyes including, biological treatment (Bessa et al., 2017; Moreira et al., 2018; Ong et al., 2020; Żur et al., 2018), photocatalysis (Ajmal et al., 2014; Castañeda-Juárez et al., 2019; Rafiq et al., 2021; Simović et al., 2023), Fenton-like processes (Qian et al., 2020; Zhang et al., 2019), membrane filtration (Alfonso-Muniozguren et al., 2021;

Liang et al., 2021; Liu et al., 2023; Pramono et al., 2023), and adsorption (Malek et al., 2021; Rostamian and Behnejad, 2018; Thakur et al., 2023; Xie et al., 2023) and others (Furlan et al., 2010; Lima et al., 2022; Wang et al., 2021). However, many of these methodologies demand expenditure of elevated costs for implementation and operation; moreover, they generate huge amounts of by-products and sludge, which require further treatments and management. However, among these methods, adsorption appears to be the most affordable, and efficient with simpler operation (Ahmed et al., 2023; Anastopoulos et al., 2022a, 2022b; Kalderis et al., 2023; Usman et al., 2022). For an effective adsorption system, the selection of the adsorbent is crucial, and activated carbon/biochar (Baccar et al., 2012; Nizam et al., 2021) is the most employed worldwide due to their high-developed porosity features and surface functional groups that are crucial characteristics for high/performance adsorbents.

Biochar can be prepared through pyrolysis from different carbon precursors, from biomass (sustainable source), which has important advantages including a low carbon footprint by using a more

---

sustainable, abundant, and low-cost source (Do Minh et al., 2020). Besides, biomass-derived carbon materials can be easily modified by doping with other chemical elements such heteroatoms and some metal oxides (Guo et al., 2020; Weidner et al., 2022). Selenium (Se), which has the same electronegativity (2.55) to the C atom is an interesting strategy for doping carbon materials. Se is a non-metallic chalcogen that possesses a large atomic size and abundant d-electron, which boost/facilitates ion/electron transport and provide additional active sites in the carbon framework (Piri et al., 2021). In addition, Se can also interact with its neighbouring molecules (Piri et al., 2021) which is helpful in attracting pollutants and boost its adsorptive properties.

Herein, Se-doped biochar was prepared using spruce bark wastes as a sustainable precursor. Norway spruce (*Picea abies* (L.) Karst.) is an important and economically valuable tree for the European forest industry. Only in Sweden, 90 Mm^3 standing volumes are harvested, which over 10–15% of this volume is bark that is undesired by-product, which possesses very low-value for industrial purposes (Jansen et al., 2017).

Se was employed as a dopant to produce a high-performance adsorbent, and the activation was done using combined hydrothermal carbonization (HTC) and pyrolysis process. The pristine biochar was used to compare the performance of Se-doped biochar. A deep investigation on the effect of Se doping over biochar's final physicochemical properties was performed through several characterization techniques such as surface area and porosity analysis, phase identification by X-ray diffraction (XRD), microscopic visualization (Scanning Electron Microscopy (SEM), and oxidation states by X-ray Photoelectron Spectroscopy (XPS). The prepared biochars were tested in the removal of two different molecules diclofenac (DCF) and reactive orange 16 dye(RO-16) dye from aqueous solutions. The adsorbents' ability to treat colourful and pharmaceuticals synthetic effluents containing several dyes and drugs contaminants were also performed. To the best of our knowledge, Se-doping biochar was never involved in the adsorption process and this work gives the first insights about using an easy and effective strategy to make Se-doped high-performative adsorbents for dyes and drugs removals, which further justifies it. Therefore, we expect that this work can open new strategies for the fabrication/development of high-performance adsorbent materials for tackling water/wastewater pollution.

2. Materials and methods

2.1. Materials

Deionized water was utilized for preparing all solution preparations. Sigma Aldrich provided the selenium dioxide (SeO$_2$), Reactive orange 16 dye (RO-16), and sodium diclofenac (DCF). All chemicals were used as received with analytical grades specified by the sender.

2.2. Carbon material preparation

The biomass carbon materials were prepared in following consecutive steps. First, 15 g of the spruce bark at a particle diameter lower than 0.5 mm were mixed with 5 g of SeO$_2$, and placed into hydrothermal carbonization (HTC) vessel of 150 mL of internal volume. 100 mL of H$_3$PO$_4$ 25% was added into the HTC vessel and heated at 150 °C for 16 h with no pressure control. After HTC treatment, the sample was placed into a beaker and dried in a drying oven for 24 h at 105 °C. After drying, the dried material was placed in a ceramic reactor and heated at 800 °C which was maintained for 1 h, under a heating rate of 10 °C/min. The sample was pyrolysed and subjected to a physical activation with CO$_2$ atmosphere under a CO$_2$ flow of 300 mL/min. The system was subsequently cooled until it reached at room temperature. After cooling, the pyrolyzed material was washed with boiling water to remove the traces of inorganics weakly attached to the carbon matrix. Subsequently, the material was dried (105 °C) and called Biochar and Biochar-Se.

2.3. Characterization of the adsorbent materials

Specific surface area (SSA), micropore area (A$_{Micro}$), mesopore area (A$_{Meso}$), and pore volume were obtained from N$_2$ isotherms measured by a sorptometer (Tristar 3000, Micromeritics Instrument Corp., Norcross, GA, USA). The adsorbent materials' surfaces were subjected to morphological analysis by using scanning electron microscopy (SEM) method through an equipment FESEM; Zeiss Merlin, using an acceleration voltage of 20 kV. XPS analysis was performed using a Kratos Axis Ultra spectrometer with Al Ka monochromated source operated at 150 W, with a pass energy of 160 and 20 eV for acquiring survey and element individual spectra. Raman spectra were obtained from a Bruker spectrometer (Ettlingen, Germany). The amorphous/crystalline feature of both biochar materials were analyzed by an Rigaku SmartLab 9 kW X-ray diffractometer (Rikagu Corporation, Tokyo, Japan), operating at 40 kV and 135 mA at a 2θ angle of 10–80 using Co as source. The software for analysis was PDXL2 coming together with the XRD device. The peaks were identified using International Centre for Diffraction Data ICDD (PDF-4 + 2023). The pH$_{pzc}$ of the biochars was determined by adding 20.00 mL of 0.050 mol/L NaCl with a previously adjusted initial pH (the initial pH (pH$_i$). The pH of NaCl solution was adjusted from 2.0 to 10.0 by adding 0.10 mol/L of HCl and NaOH to several 50.0 mL falcon tubes containing 50.0 mg of biochars (Biochar and Se-Biochar in separate tubes). The suspensions were shaken in an acclimatized shaker at 298 K and allowed to equilibrate for 48 h. The suspensions were then centrifuged at 10,000 rpm for 10 min to separate the biochars from the
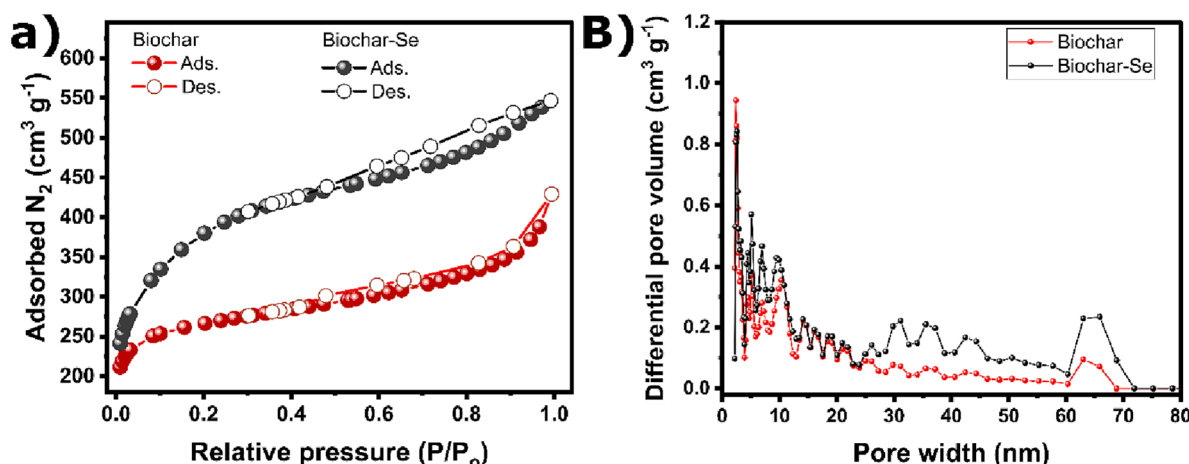
Fig. 1. a) N$_2$ isotherms of adsorption-desorption and b) pore size distribution curves of Biochar and Biochar-Se.

Table 1
Porosity features of the biochar materials.

	SSA	A_{Micro}	A_{Meso}	Mesoporosity	Pore volume
	$(m^2\ g^{-1})$			(%)	$(cm^3\ g^{-1})$
Biochar	1207	402	805	66.7	0.84
Biochar-Se	1300	371	929	71.5	0.83

aqueous solution. The pH_i of the solutions was accurately measured using the solutions that had no contact with the solid adsorbents; the final pH (pH_f) values of the supernatant after contact with the solid were recorded. The value of pH_{pzc} is the point where the curve of pH (pH_f − pH_i) versus pH_i crosses a line equal to zero.

2.4. Adsorption studies

The batch adsorption was employed to test the ability of Biochar and Biochar-Se in adsorbing RO-16 and DCF from synthetic solutions. The mass effect, pH effect, contact time, and initial dye and drug concentration were subjected to a deep evaluation. The adsorption tests were performed in 50.0 mL Falcon tubes containing 20 mL of solution. The pH effect was studied at pH range from 2 to 10. The kinetic was performed using a fixed DCF and RO-16 solution concentrations of 200 mg L^{-1}, and with a contact time from 0 to 360 min. For isotherms experiments, both DCF and RO-16 molecules ranged their initial concentrations from 50 to 1200 mg L^{-1}. The adsorption tests were fixed at a shaking speed of 250 rpm for all experiments. After the contact time, the treated solutions of DCF and RO-16 were measured by UV–Visible spectrophotometry technique at wavenumbers of 276 nm (DCF) and 494 nm (RO-16). The capacity of removal in q and % for both molecules were determined based on Eqs 1 and 2, respectively, described in the supplementary material.

3. Results and discussion

3.1. Physicochemical characterization of the materials

The porosity structure including BET surface area, micropore and mesopore structures, and pore volume are essential features to understand the efficiency of the biochars in the adsorption process, including the mechanism of adsorption. The N_2 isotherms were performed to obtain the porosity features of Biochar and Biochar-Se. The N_2 isotherm curves (See Fig. 1a) confirmed the highly porous materials' characteristics. Based on IUPAC classification, both isotherms can be classified as type IV, which exhibit a hysteresis loop suggesting high presence of

mesopores (dos Reis et al., 2021; Thommes et al., 2015). However, under low partial pressure, a high N_2 uptake is observed, which is attributed to the presence of microporous in the carbon pore structures. Corroborating with N_2 curves, the pore size distribution curves of the carbon materials are exhibited in Fig. 1b. It can be seen that large fractions are at diameter of around 2 nm (due to the micropores indicated in N_2 isotherms). In addition, big fractions of pores with diameters up to 10 nm (small mesopores) are clearly seen in both materials.

However, Biochar-Se shows more mesopore features in the range from 25 to 50 nm (big mesopores), and some presence of macropore (around 75 nm). It seems that the selenium doping enhanced the number of mesopores in the biochar. This statement is corroborated by the data presented in Table 1, which shows SSA, micro and mesopore areas, and mesoporosity contribution. The obtained areas were 1207 and 1300 m^2/g, for non-doped and Biochar-Se, respectively. The enhancement in SSA value from Biochar to Biochar-Se sample highlights that the Se can act as a spacer, due to its large atomic size, which widens the small pore into bigger ones. In addition, it is known that the introduction of heteroatoms including Se induces the creation of defects in the carbon structure, which serves as active adsorption sites for boosting the material's adsorptive performance (dos Reis et al., 2023a).

The morphology of Biochar and Biochar-Se was analysed using SEM to ascertain the impact of Se-doping on the materials. SEM images correspond to Biochar (Fig. 2a,b,c) and Biochar-Se (Fig. 2d,e,f). The SEM images were obtained at different magnifications 5 K (Fig. 2a,d), 55 K (Fig. 2b,e) and 150 K (Fig. 2c,f). It is clear from SEM images (Fig. 2) that Se doping had a remarkable impact on surface morphology of biochar. Pure biochar seems to present an intact structure with a smoother surface with no cracks or holes (Fig. 2a). However, going to a 55KX of magnification (Fig. 2b), the surface of Biochar sample displays some roughness what is further confirmed by observing the Fig. 2c (150 K of magnification). Compared to pure biochar, Biochar-Se presented a much rougher and lesser intact surface (Fig. 2d,e,f), what can be related to the effect of selenium doping that created more physical defects on the doped biochar. Carbon materials rich in defects are reported to be suitable adsorbent materials because the defects can act as adsorptive sites (He et al., 2023; Wang et al., 2022).

Fig. 2 also shows the Selenium EDS element mapping is shown in (Fig. 2d, insert), which revealed a homogeneous distribution of this element over the biochar structure; the quantitative EDS analysis showed that roughly 2% of Se was introduced in the carbon structure, proving the successful Se-doping.

The elemental composition and chemical bonding states biochar adsorbent materials were evaluated through XPS method and its spectra
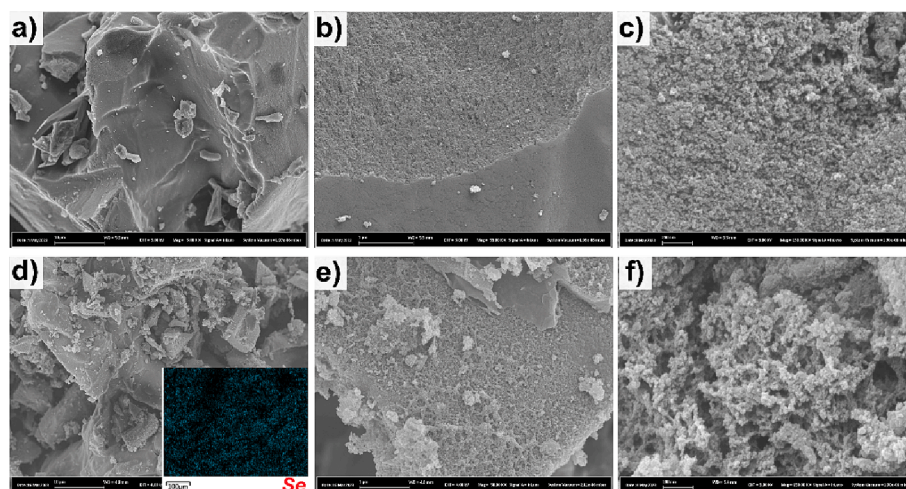
Fig. 2. SEM images of materials: a) Biochar at 5 K of magnification; b) Biochar at 55 K of magnification; c) Biochar at 150 K of magnification; d) Biochar-Se at 5 K of magnification with EDS mapping of selenium; e) Biochar-Se at 55 K of magnification; f) Biochar-Se at 150 K of magnification.
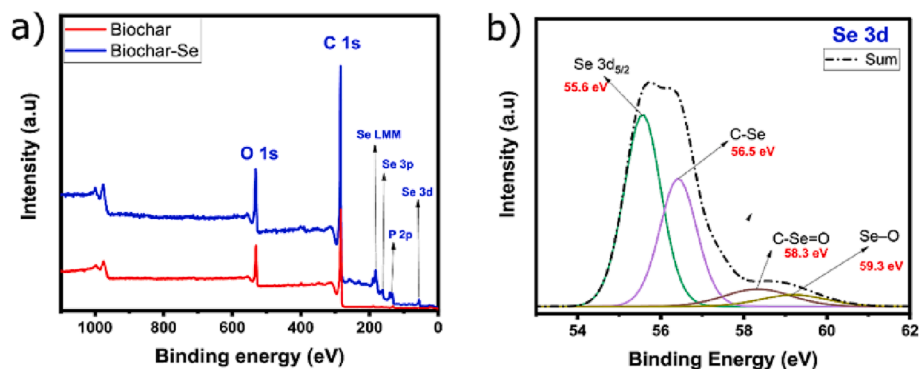
Fig. 3. a) XPS survey spectra of Biochar and Biochar-Se and b) deconvoluted Se 3d peaks.
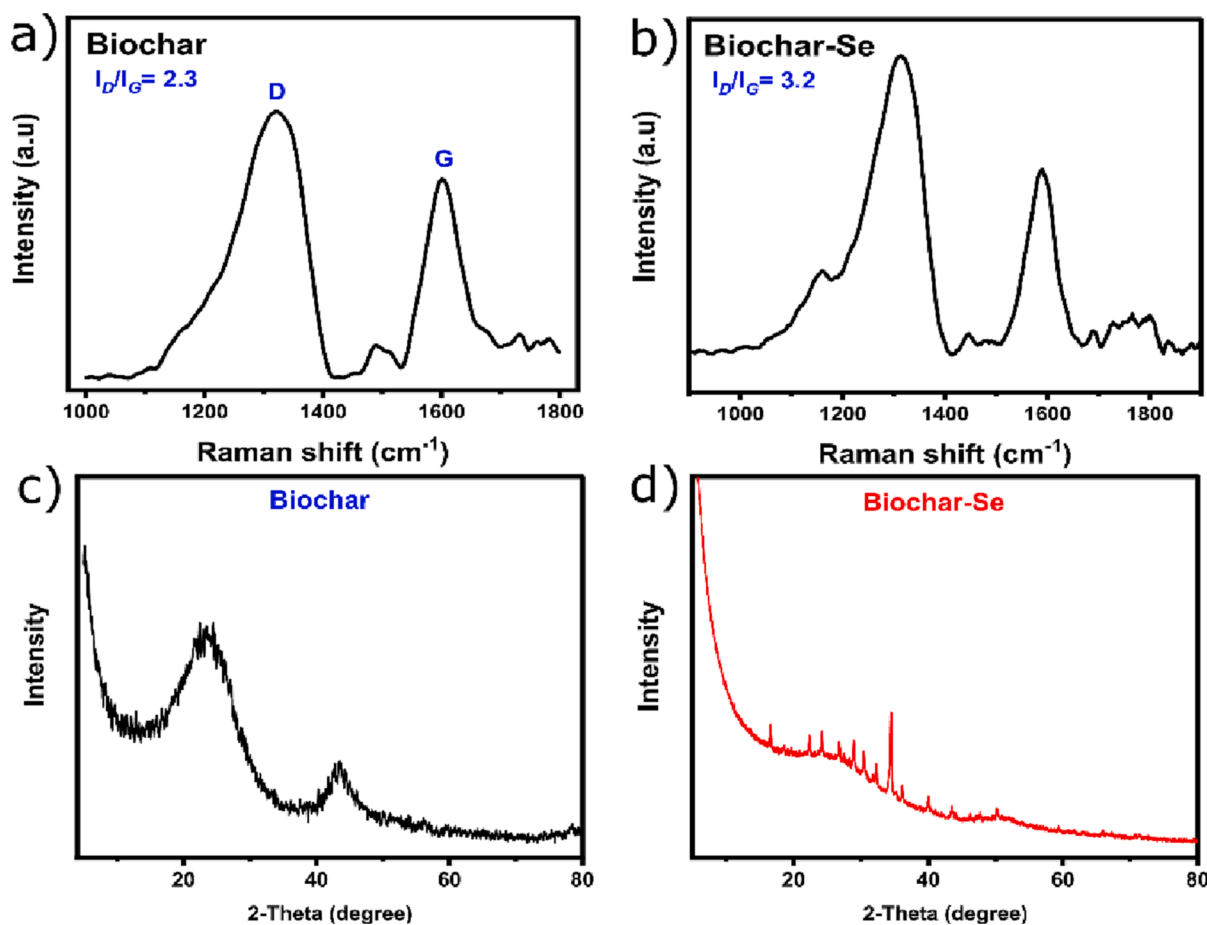
Fig. 4. Raman spectra of Biochar (a) and Biochar-Se (b), and XRD patterns for Biochar (c) and Biochar-Se (d).

are shown in Fig. 3. The XPS survey spectra (Fig. 3a) of Biochar and Biochar-Se indicate the presence of carbon, oxygen, and phosphorus in both materials while Se is observed only in Biochar-Se indicating its successful doping. It is worthwhile to note that the phosphorus present in both biochars is in PO_4^{3-} form, and it comes from H_3PO_4 that was used to chemically activate the biochars. The Se 3d deconvoluted XPS data of Biochar-Se is shown in Fig. 3b and it exhibits similar to those of Se-doped carbon in the literature (B. Zhang et al., 2020). The Se 3d peaks at 55.6 eV and 56.5 eV are ascribed to Se 3d5/2 and Se 3d3/2, representing the selenium-carbon bond (Jin et al., 2012) while the peaks at 58.3 and 59.5 eV are attributed to selenium bonded to oxygen (Liu et al., 2020; Luo et al., 2015). The quantitative values for carbon, oxygen, phosphorus and selenium for Biochar-Se were 86.5, 10.8, 1.80 and 1.10% (at. ratio

%), while for Biochar were 87% (carbon), 8.9% (oxygen), and 1.2% (phosphorus) (see supplementary Table S3). Se was not detected in Biochar sample. The XPS results showed that Biochar-Se nanostructure contains selenium, indicating the formation of C-Se chemical bonds in the carbon frameworks.

Raman spectroscopy is a widely informative technique for the evaluation of the microstructure of the materials in terms of degree of order/ disorder/graphitization (González-Hourcade et al., 2022; Piergrossi et al., 2019; Yang et al., 2019). The above discussed characterization data have proved the successful incorporation of Se in the biochar structure. To further investigate the structural changes of Se-doping on biochar characteristics, Raman analysis was accessed (Fig. 4a,b). It can be observed two peaks at 1,340 cm^{-1} and 1,600 cm^{-1}, characteristics of
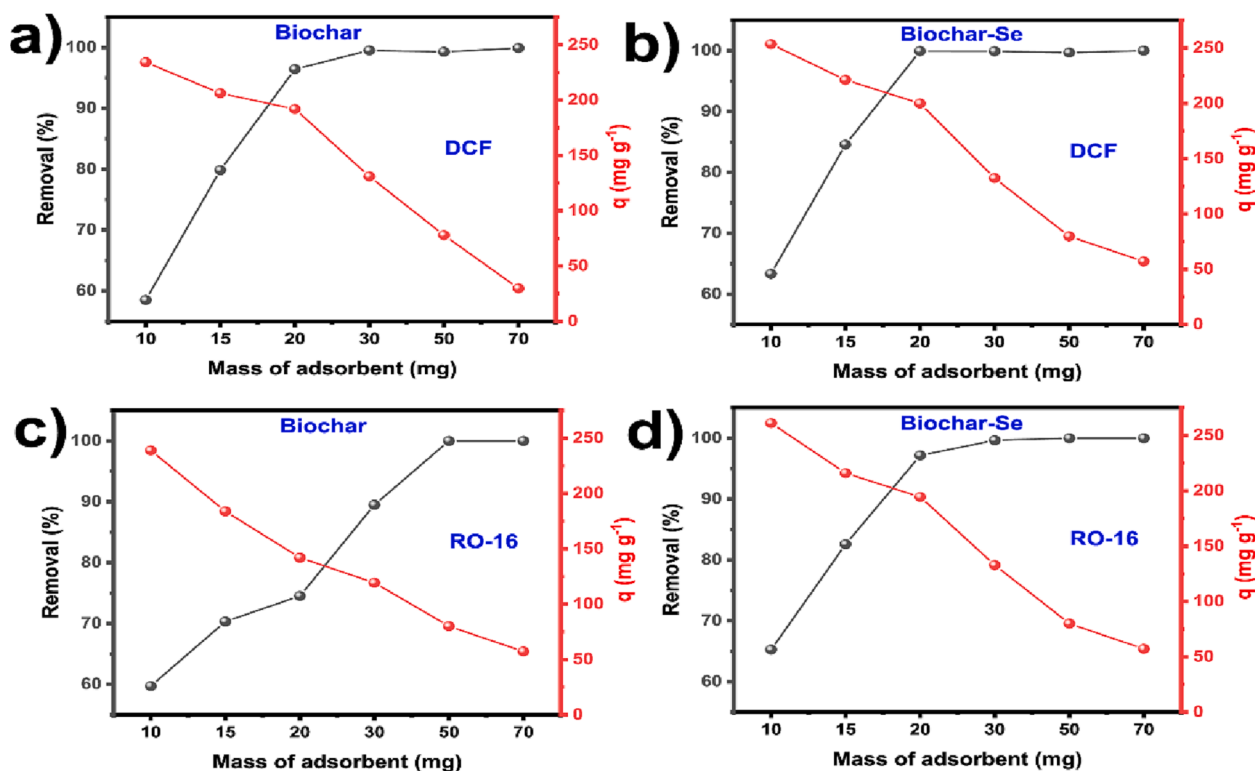
Fig. 5. Mass effect on DCF and RO-16 removal: a) Effect of Biochar mass on DCF removal; b) Effect of Biochar-Se mass on DCF removal; c) Effect of Biochar mass on RO-16 removal; and d) Effect of Biochar-Se mass on RO-16 removal.

defect and graphite structures, respectively. The peak related to defect (D-peak, 1,340 cm^{-1}) is attributed to carbon atoms rich in defects/disordered structures that is dominant in biochar with amorphous feature (dos Reis et al., 2022a, 2023a). The peak at 1,600 cm^{-1} that corresponds to graphitic C atoms with sp^2 electronic configuration (Pawlyta et al., 2015; Piergrossi et al., 2019).

From Raman spectrum, the intensity of the D and G peaks can be calculated based on its areas, and the ratio between D and G bands (I$_D$/I$_G$) is widely studied to evaluate the level of material's graphitization (Piergrossi et al., 2019; Yang et al., 2019). The I$_D$/I$_G$ values for Biochar and Biochar-Se were 2.3 and 3.2, respectively, which implied that Se-doping enabled the creation of disorder/imperfection structure in the Biochar-Se carbon lattice. As already mentioned, an adsorbent rich in defects can have its adsorptive performance boosted, thus Se-doping was an efficient strategy for the preparation of suitable biomass adsorbent materials.

The amorphous/crystalline structure of the pristine biochar and Biochar-Se materials were examined by XRD shown in Fig. 4,c and d. The XRD pattern for the pristine biochar show two broad peaks. One higher peak at around 2θ of 22° which can be attributed to amorphous carbon structures C (0 0 2), and a weaker peak at 2θ of 40-50° may attributed to graphite structures, these two peaks are matching well with characteristic carbon-based peaks (Xie et al., 2023; Omorongie et al., 2021). On the other hand, the XRD patterns for Biochar-Se showed many crystallite peaks. The two broad amorphous C peaks can be observed also at 2θ of 22° and 50°. The peaks at 2θ of 26.8°, 32.4°, 36.1° and 50.2° are match to Se (ICDD 04-009-6204). The peaks at 2θ of 28.9° and 34.5° are match with SeC$_4$O$_2$ (ICDD 04-013-9181). The peaks at 2θ of 22.4° and 30.4° are match to SeO$_3$ (ICDD 04-007-1435). The graphite carbon peak exhibits at 2θ of 30.4° which is overlapping with SeO$_3$ peak. The peaks at 2θ of 24.2° and 36.1° are match with P$_2$O$_5$ (ICDD 01-071-6182) as phosphoric acid, which was used for the biochar activation during
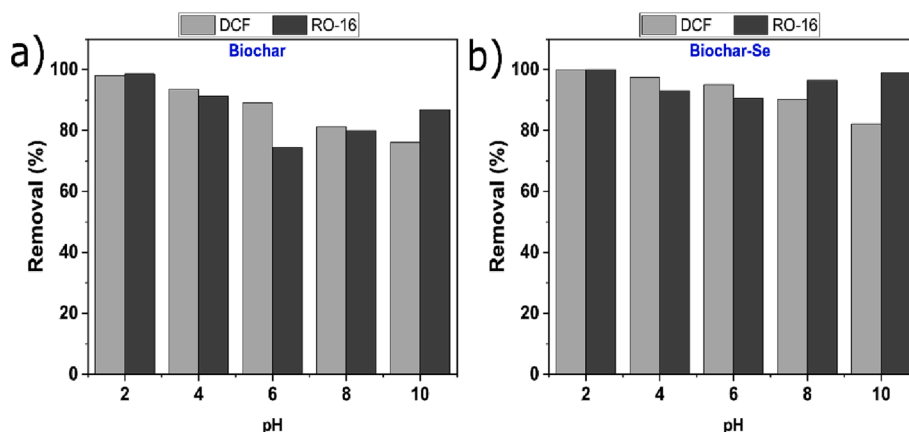
Fig. 6. The effect of pH on DCF and RO-16 removal.
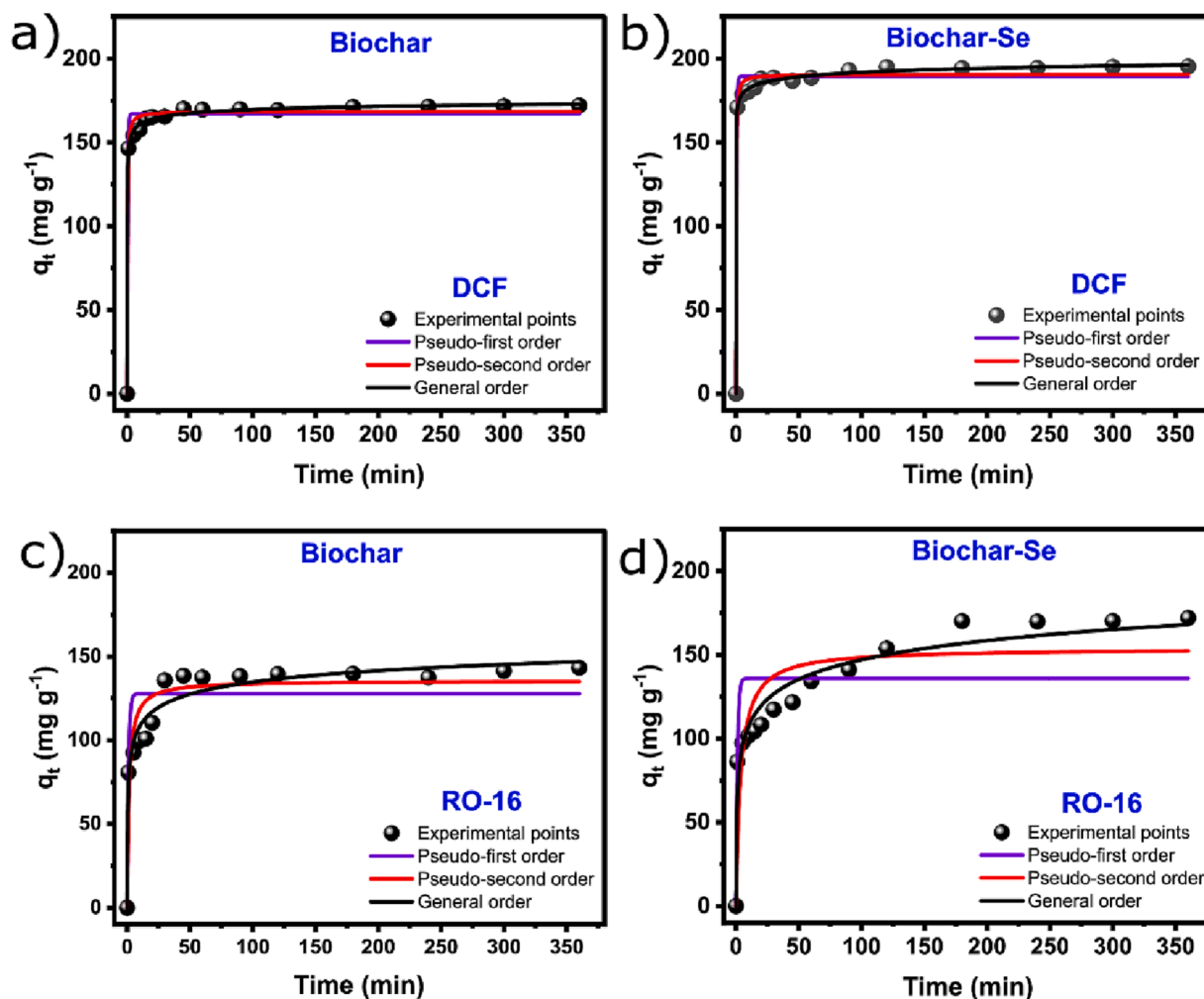
Fig. 7. Kinetics of adsorption curves at 298 K for DCF (a,b) and RO-16 (c,d) on Biochar and Biochar-Se. Conditions: initial pH 6 and adsorbent dosage of 1 g /L.

HTC. The peak at 2θ of 16.6°and 40.1° are match to Se_5S_2 (ICDD 04-007-0631) denote trace impurity of Sulfur.

The XRD results indicate the successful introduction of Se nanoparticles in Biochar-Se. The Se is partly oxidized and bonded with C as well. Moreover, it also indicates that Se nanoparticles were highly dispersed in Biochar carbon matrix yielding a crystalline structure.

3.2. Adsorption studies

3.2.1. Mass effect on DCF and RO-16 adsorption

In an adsorption process, the quantity of adsorbent (in mass) is a very important factor to evaluate its efficiency and industrial applicability. Moreover, the study of the mass of the adsorbent is also important to avoid waste generation and reduce costs associated with the adsorbent application during the adsorption process. Fig. 5 displays the influence of the adsorbent mass on DCF and RO-16 removal with mass amounts ranging from 10 to 70 mg in 20 mL of adsorbate solution. The curves display that Biochar-Se exhibited better results with lower mass amounts than pristine Biochar. For instance, for DCF with 20 mg of Biochar, 96% of removal was achieved while Biochar-Se removed almost 100%. For RO-16 the same trend was observed, with 20 mg of adsorbents, pristine biochar removed 74% while Biochar-Se removed 97%. The better performance of Se-doped biochar can be the fact that the doping process introduced more active sites that improve the adsorptive skills of the Biochar-Se. for the subsequent adsorption tests, a mass of 20 mg was fixed (an adsorbent dosage of 1 g/L).

3.2.2. pH effect on DCF and RO-16 adsorption

The pH of the solution is one of the most influential factors affecting the adsorption process because it affects the speciation of the adsorbates and therefore its ability to bind adsorbents surfaces (Iftekhar et al., 2018; Yang et al., 2019). The pH effect on DCF and RO-16 removal was evaluated in the pH range of 2–10, and the results are shown in Fig. 6. It is observed that acidic conditions favoured both DCF and RO-16 adsorption on both adsorbents. It is widely reported that the pH influences the chemical speciation of DCF and RO-16, and different molecule structures can be obtained considering their pKa value (Bagal and Gogate, 2014; de Azevedo et al., 2023; Kheradmand et al., 2022; Naddeo et al., 2010). DCF exists in its molecular form when the pH is lower than its pKa value (4.35 ± 0.2). However, ionic form of DCF is predominant when the pH values greater than the pK_a value (Bagal and Gogate, 2014; Naddeo et al., 2010). Since the RO16 structure has hydroxyl groups, these groups form hydrogen bonds with the adsorbent's OH sites. RO 16 pKa value is 11.23 and dye ionizes into anion form at lower pH and affects electrostatic interaction with the charged adsorbent surface (Kheradmand et al., 2022).

The point of zero charge (pH$_{pzc}$) is an important measurement for determination of the charge of an adsorbent, which helps to understand the interaction between adsorbent and adsorbate. The pH$_{pzc}$ of the biochar materials was performed to obtain the point that indicates where the material's surface charges is equal to zero, which below this point, the surface charge is positive and above is negative. Supplementary Fig. S1 shows the pH$_{pzc}$ for Biochar and Se-Biochar. The Se-Biochar exhibited a pH$_{pzc}$ of 2.3 which is lower than of that exhibited by the

Table 2
Kinetic model parameters for DCF and RO-16 adsorption.

DCF	Biochar	Biochar-Se
Pseudo-first order		
q_1 (mg g^{-1})	167.0	189.0
k_1 (min^{-1})	2.100	2.331
R_{adj}^2	0.9841	0.9870
SD (mg g^{-1})	5.400	5.630
Pseudo-second order		
q_2 (mg g^{-1})	168.0	191.0
k_2 (g mg^{-1} min^{-1})	0.03310	0.03830
R_{adj}^2	0.9912	0.9915
SD (mg g^{-1})	4.041	4.580
General order		
q_n (mg g^{-1})	182.0	339.1
k_n (min^{-1} (g mg^{-1})$^{n-1}$)	6.4×10^{-8}	2.3×10^{-20}
n (-)	5.201	11.52
$t_{95\%}$ (min)	22.19	26.12
R_{adj}^2	0.9991	0.9999
SD (mg g^{-1})	1.751	1.603
RO-16	**Biochar**	**Biochar-Se**
Pseudo-first order		
q_1 (mg g^{-1})	128.3	136.1
k_1 (min^{-1})	0.9102	0.9104
R_{adj}^2	0.7901	0.6234
SD (mg g^{-1})	17.93	17.70
Pseudo-second order		
q_2 (mg g^{-1})	136.2	154.0
k_2 (g mg^{-1} min^{-1})	0.005112	0.001822
R_{adj}^2	0.8821	0.7630
SD (mg g^{-1})	13.1	12.87
General order		
q_n (mg g^{-1})	155.1	178.3
k_n (min^{-1} (g mg^{-1})$^{n-1}$)	3.1×10^{-11}	7.1×10^{-16}
n (-)	9.971	37.50
$t_{95\%}$ (min)	160.0	190.2
R_{adj}^2	0.9524	0.9702
SD (mg g^{-1})	8.422	10.13

pristine biochar (4.3). pH < pH$_{pzc}$, it would be favorable for the RO-16 anionic dye adsorption (dos Reis et al., 2023b). This is highlighted in Fig. S1 which shows higher removals of RO-16 at lower pHs. The removal of DCF showed the same trend of having its higher removals at lower pHs (see Fig. S1). When the pH value was higher than the pH$_{pzc}$, the adsorption decreased due to the electrostatic repulsion between the negative charge on the biochars' surfaces and the negative charge on DCF molecules (Xie et al., 2023; Liu et al., 2013). However, it is noted that the decrease in the adsorption was not so high which demonstrated that the electrostatic interactions were not the main mechanism involved in the adsorption process. Similar behaviour was observed in the case of RO-16 dye.

3.2.3. Kinetic study

The adsorption rate provided by the kinetic of adsorption is an important information to understand the efficiency and practicability of an adsorbent and to better design a high-effective adsorption process (Lima et al., 2015; Yu et al., 2021). Fig. 7 and Table 2 show the kinetic curves and parameters for both DCF and RO-16 removals on both carbon materials. Similar behaviour for both molecules on both adsorbents, an extremely rapid uptake for both DCF and RO-16 at the very first minute for both adsorbents is observed, which gradually seems to reach the equilibrium within 45 min. The fast uptake at the beginning of the kinetic can be attributed to the many available active adsorption sites available on the biochar adsorbents that easily adsorb DCF and RO-16 molecules, and plateau, which is related to the equilibrium process due to the saturation of these active adsorbent sites.

The kinetic study was deeply evaluated by the fitness of three kinetic models, including pseudo-first-order, pseudo-second-order, and General order (Fig. 7 and Table 2). The models' suitability was statistically evaluated through R2$_{adj}$ and SD values (Cimirro et al., 2022; dos Reis et al., 2022a; Dotto et al., 2023; González-Hourcade et al., 2022) (see

Supplementary Material). The model that possesses the highest R$_{adj}^2$ and lowest SD values is the one with the best fitness of experimental data. This statistically means that the experimental and theoretical q values (obtained from the models) have smaller differences (Cavalcante et al., 2022; dos Reis et al., 2022b). In this sense, general order exhibited the best fitness for the experimental results for both adsorbate molecules (DCF and RO-16) on Biochar and Biochar-Se adsorbents because it exhibited the highest R$_{adj}^2$ and lowest SD values.

General order is a widely employed model to study the kinetic of adsorption process and its suitability means that the order of adsorption process should be the same as that of a chemical reaction, in which the reaction kinetic order is measured experimentally (Bergmann and Machado, 2015; Lima et al., 2015). However, General order displays different n values when the adsorbates (DCF and RO-16) initial concentrations are varied making extremely complex the comparison between the constant kinetic rates (k$_N$) (Cavalcante et al., 2022).

Therefore, $t_{95\%}$ can be easily explored to compare the kinetics of adsorption of DCF and RO-16 on Biochar and Biochar-Se. $t_{95\%}$ is the time to attain 95% of the total saturation provided by the best fitted kinetic model (Cavalcante et al., 2022; dos Reis et al., 2022b). T$_{95\%}$ values show that the adsorption of both molecules were faster for Biochar compared to Biochar-Se, and the adsorption of DCF was much faster than RO-16 (See Table 2). The faster adsorption of DCF highlights its more affinity compared to RO-16, which could be explained based on its physical features of these two molecules. For instance, DCF has a smaller size (1.012 nm) compared to RO-16 (1.68 nm); in addition, the molecular weight of the DCF is 318.1 g mol^{-1} while RO-16 is 617.7 g mol^{-1} (almost twice the size of DCF). Smaller molecules are easily and faster diffused into the adsorbent pores and this could explain why DCF was faster than RO-16.

Thus, in order to continue the equilibrium tests, the contact time for the subsequent tests was fixed at 40 min for DCF and 200 min for RO-16 to ensure that the contact times were sufficient for attaining equilibrium.

3.2.4. Equilibrium study

To obtain the equilibrium study of an adsorption system is crucial to properly understand the relationship between an adsorbate (e.g., DCF and OR-16) at different initial concentrations and its degree of accumulation onto adsorbent surface at a constant temperature. Moreover, the equilibrium study is essential to have important insights over the adsorption mechanism, affinity and adsorbent's surface properties. In the literature, there are several isotherm models used to describe the equilibrium in adsorption processes but in this work Langmuir, Freundlich and Liu models were employed to evaluate the equilibrium data.

The isotherm curves and parameters are shown in Fig. 8 and Table 3. The suitability of the equilibrium models was evaluated as the same as the kinetic studies (from R$_{adj}^2$ and SD values). Observing that Liu model exhibited the lowest SD and highest R$_{adj}^2$ values, it is possible to state that statistically, Liu model presented the best fitness for both molecules (DCF and RO-16) on both adsorbent materials (see Table 3). The Liu model assumes that the adsorbent's adsorption active sites do not possess the same energy. Therefore, the adsorbents may present active sites preferred by both molecules (DCF and RO-16) for occupation. However, under the explored conditions, Freundlich exhibited the second most suitable isotherm model, indicating a more heterogeneous adsorption for both adsorbents and molecules, with different energy adsorption sites.

3.2.5. Comparison of adsorptive properties of the Se-Biochars with other adsorbents reported in the literature

The adsorption data have shown that Biochar and Biochar-Se exhibited very good affinity for adsorbing DCF and RO-16 from aqueous solutions. Nevertheless, in order to assess their efficacy, they were subjected to a comparison with different adsorbents, reported by previous researchers (Table 4). For an easy comparison, it is assumed that
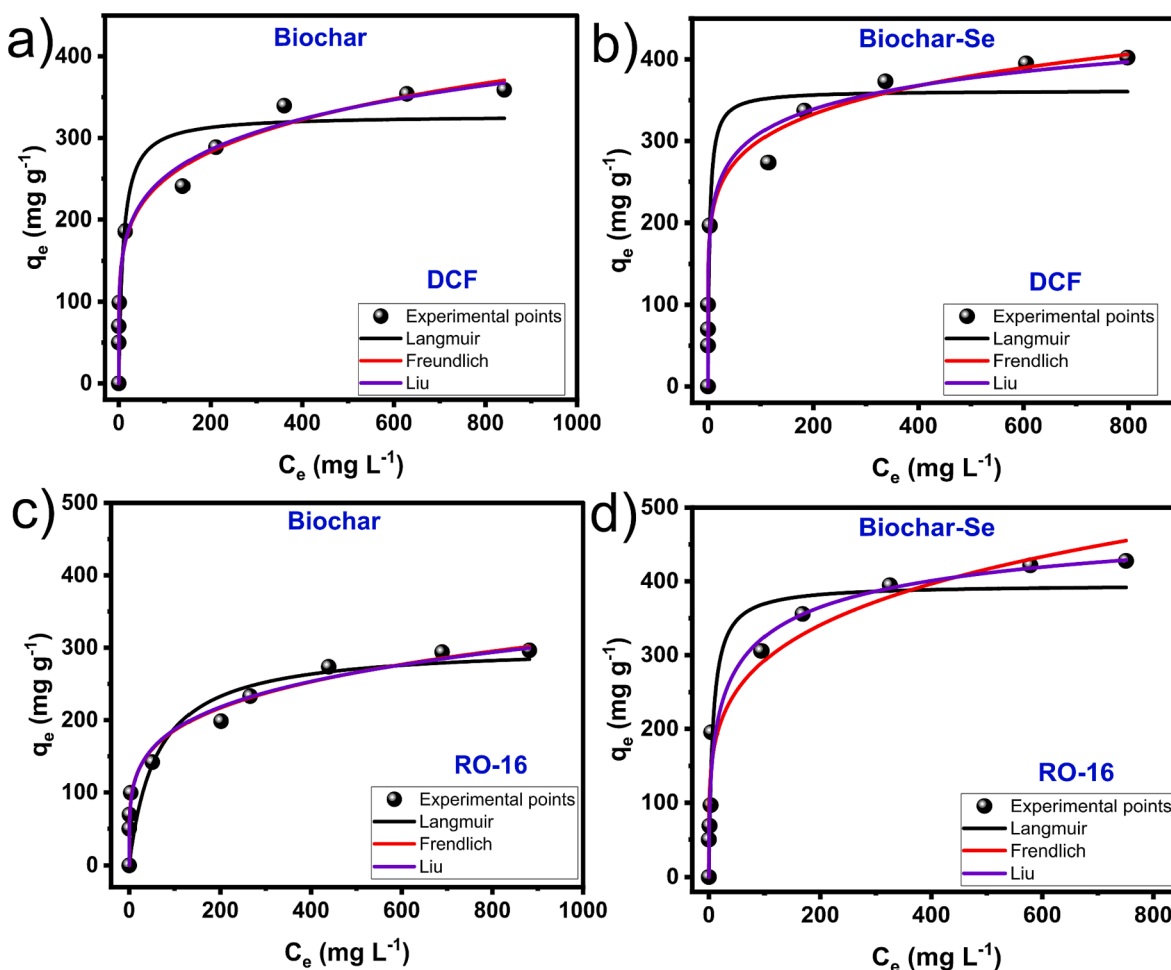
Fig. 8. Equilibrium curves at 298 K for DCF (a,b) and RO-16 (c,d) on Biochar and Biochar-Se. Conditions: initial pH 6, contact time of 40 min (DCF) and 200 min (RO-16), and adsorbent dosage of 1 g/L.

Table 3
Isotherm equilibrium model parameters for DCF and RO-16 adsorption.

	Biochar	Biochar-Se	Biochar	Biochar-Se
Langmuir	**DCF**		**RO-16**	
q_e (mg g^{-1})	328.3	362.0	304.2	395.3
k_1 (L mg^{-1})	0.1003	0.3221	0.01611	0.1412
R^2_{adj}	0.8731	0.8642	0.8332	0.9552
SD (mg g^{-1})	40.12	58.32	44.41	38.44
Freundlich				
k_F ((mg g^{-1}) (mg L^{-1})$^{-1/nF}$)	105.2	155.1	66.74	107.2
n_F (dimensionless)	5.344	6.974	4.503	4.570
R^2_{adj}	0.9444	0.9123	0.9640	0.9550
SD (mg g^{-1})	33.41	48.72	21.69	36.12
Liu				
Q_{max} (mg g^{-1})	354.7	434.0	331.8	538.1
K_g (L mg^{-1})	0.005699	0.09688	0.001402	0.02399
n_L (dimensionless)	0.1006	0.2197	0.2211	0.4704
R^2_{adj}	0.9600	0.9321	0.9698	0.9701
SD (mg g^{-1})	30.12	42.10	18.19	31.41

that the data in Table 4 were obtained under optimum adsorption conditions. In this sense, Biochar-Se shows to be very competitive and efficient for the uptake of both molecules (DCF and RO-16) when compared to other adsorbent materials displayed in Table 4. Some of the adsorbents, including those based on ground nut shells and sawdust, demonstrated the removal of dyes, but the pH was extremely low, requiring the use of additional chemicals to maintain pH (Muralikrishnan and Jodhi, 2021; Shah et al., 2020).

Analyzing the data in Table 4, it is seen that two adsorbents had better performances than Biochar-Se, Cyclamen persicum tubers based activated carbon (Jodeh et al., 2016) and Chitosan tripolyphosphate/TiO$_2$ nanocomposite (Abdulhameed et al., 2019); however, despite having higher q$_{max}$, it is crucial to highlight that Chitosan tripolyphosphate/TiO$_2$ nanocomposite has much more complex synthesis method, which implies in much higher costs, which could not justify their real scale application. In contrast, Biochar-Se can be made from an abundant, natural, low-cost precursor with enormous potential for real application.

3.2.6. Proposed mechanism of adsorption
On the basis of the adsorption data obtained in this research, possible mechanism interactions between Biochar-Se and DCF and RO-16 were proposed (See Fig. 9). A common explanation for the possible mechanisms of adsorption between metal-doped porous biochars and organic pollutants (adsorbates) include electrostatic interaction, hydrogen interaction, π-π interaction, and interaction among metal particles and carbon materials (Feiqiang et al., 2018; Kazeem et al., 2018). Also, since both materials are very porous, pore filling is one of the main mechanism involved in both adsorbates. Cationic metal-doped carbon materials and anionic dyes attract each other by electrostatic forces to form chemical bonds. Also, the phosphate groups can attact the DFC and RO-16 molecules. π-π interaction is basically involved between the aromatic rings of Biochar-Se and aromatic rings of DCF and RO-16 molecules. H-bonding occurs between atoms (e.g., O, H, N) present in Biochar-Se and adsorbate molecules (DCF and RO-16) that tend to form H bonds. The metal doping on the carbon matrix also creates synergic effects that

Table 4

Comparison of the q_{max} for reactive orange 16 dye and sodium diclofenac using different adsorbents.

Adsorbents	Adsorbate	q_{max} (mg g^{-1})	Isotherm Model	T (°C)	pH	Adsorbent dosage (g L^{-1})	Refs.
MnFe2O4 functionalized magnetic sawdust-based biochar	DCF	344.26	Sips	25 °C	4.0	0.15	(Zhang et al., 2022)
Aquatic plant-derived biochars	DCF	23.25	Langmuir	20 °C	6.0	0.12	(Xu et al., 2020)
Cyclamen persicum tubers based activated carbon	DCF	606.78	Freundlich	15 °C	2.0	14	(Jodeh et al., 2016)
Anthriscus sylvestris-derived activated biochar	DCF	392.9	Langmuir	35 °C	6.0	0.25	(Shirani et al., 2020)
Biochar from waste sludge/leaf	DCF	287.81	Temkin	25 °C	6.5	6.25	(Zhang et al., 2020)
MgAl/layered double hydroxide supported on Syagrus coronata biochar	DCF	168.04	Sips	60 °C	5.0	0.05	(de Souza dos Santos et al., 2020)
Biomass of Ulva Prolifera	RO-16	232.0	Langmuir	45 °C	2.0	2.0	(Ravindiran et al., 2022)
Psyllium seed powder	RO-16	206.6	Langmuir	30 °C	4.0	2.0	(Malakootian and Heidari, 2018)
Melia Azedarach waste sawdust	RO-16	58.54	Langmuir	30 °C	2.0	1.0	(Shah et al., 2020)
Groundnut shell, Arachis hypogaea	RO-16	11.05	Freundlich	30 °C	2.0	1.0	(Muralikrishnan and Jodhi, 2021)
Activated carbon from Brazilian-pine fruit shell (AC-PW)	RO-16	472	Sips	50 °C	6.0	0.4	(Calvete et al., 2010)
Chitosan tripolyphosphate/TiO$_2$ nanocomposite (CCTPP/ TiO$_2$ NC)	RO-16	618.7	Freundlich	40 °C	4.0	1.8	(Abdulhameed et al., 2019)
Chitosan-polyvinyl alcohol/fly ash (m-Cs-PVA/FA)	RO-16	123.8	Freundlich	30 °C	4.0	0.6	(Malek et al., 2021)
Biochar	RO-16	332	Liu	25 °C	6.0	1.0	This work
Biochar	DCF	355	Liu	25 °C	6.0	1.0	This work
Biochar-Se	RO-16	538	Liu	25 °C	6.0	1.0	This work
Biochar-Se	DCF	434	Liu	25 °C	6.0	1.0	This work
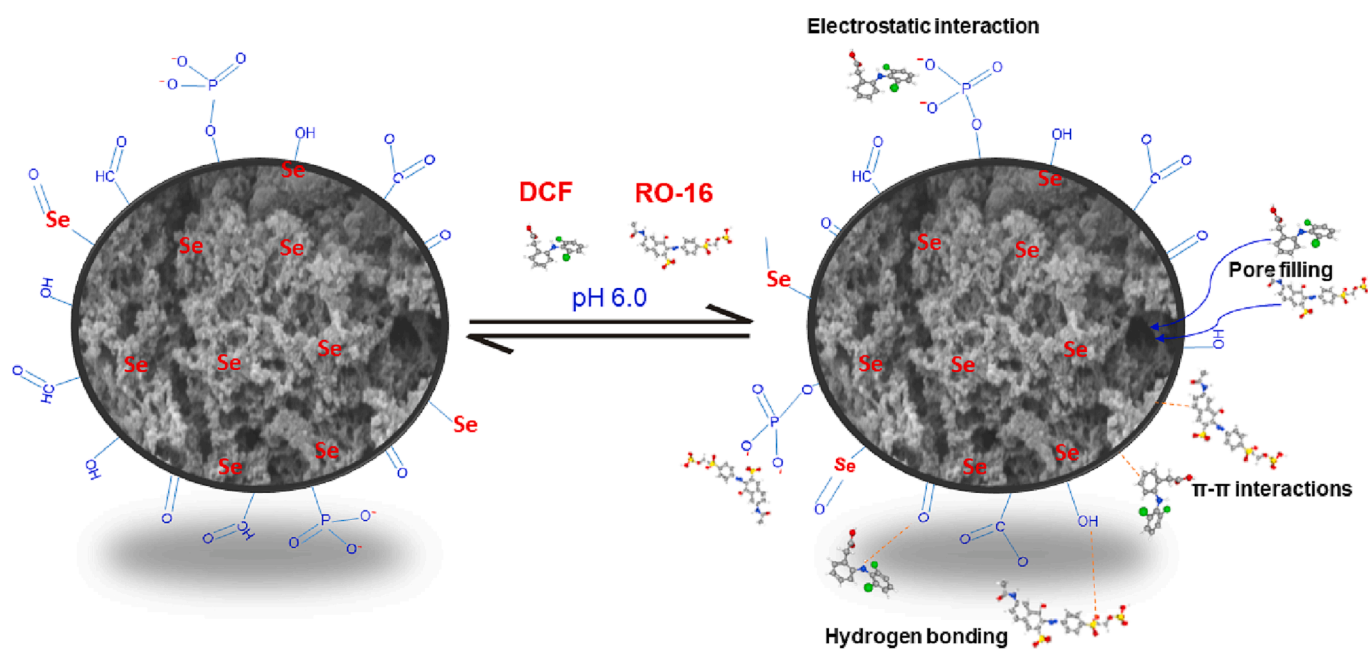
Fig. 9. Proposed mechanism of adsorption involved in the DCF and RO-16 adsorption onto Se-doped biochar.

boost the adsorption of DCF and RO-16 (Feiqiang et al., 2018; Kazeem et al., 2018). The introduction of Se-nanoparticles can interact with oxygen funcionalities present on the surface of biochar to form the metal–oxygen bond, which creates physicochemical and electronic changes/defects on adsorbent's surface resulting in the metal–oxygen bond easier to binding DCF and RO-16 molecules (Feiqiang et al., 2018; Kazeem et al., 2018).

3.2.7. Synthetic effluent treatment

The adsorption results have proved that the prepared adsorbents were very efficient in removing a single molecule (DCF or RO-16) from aqueous solution. However, in this section, the adsorbents (Biochar and Biochar-Se) were subjected to treat 4 different synthetic wastewaters (carried with several dyes, drugs, and inorganic compounds, See supplementary Table S1 and Table S2). Which means that if the materials are efficient in treating the synthetic effluents it could also be efficient in
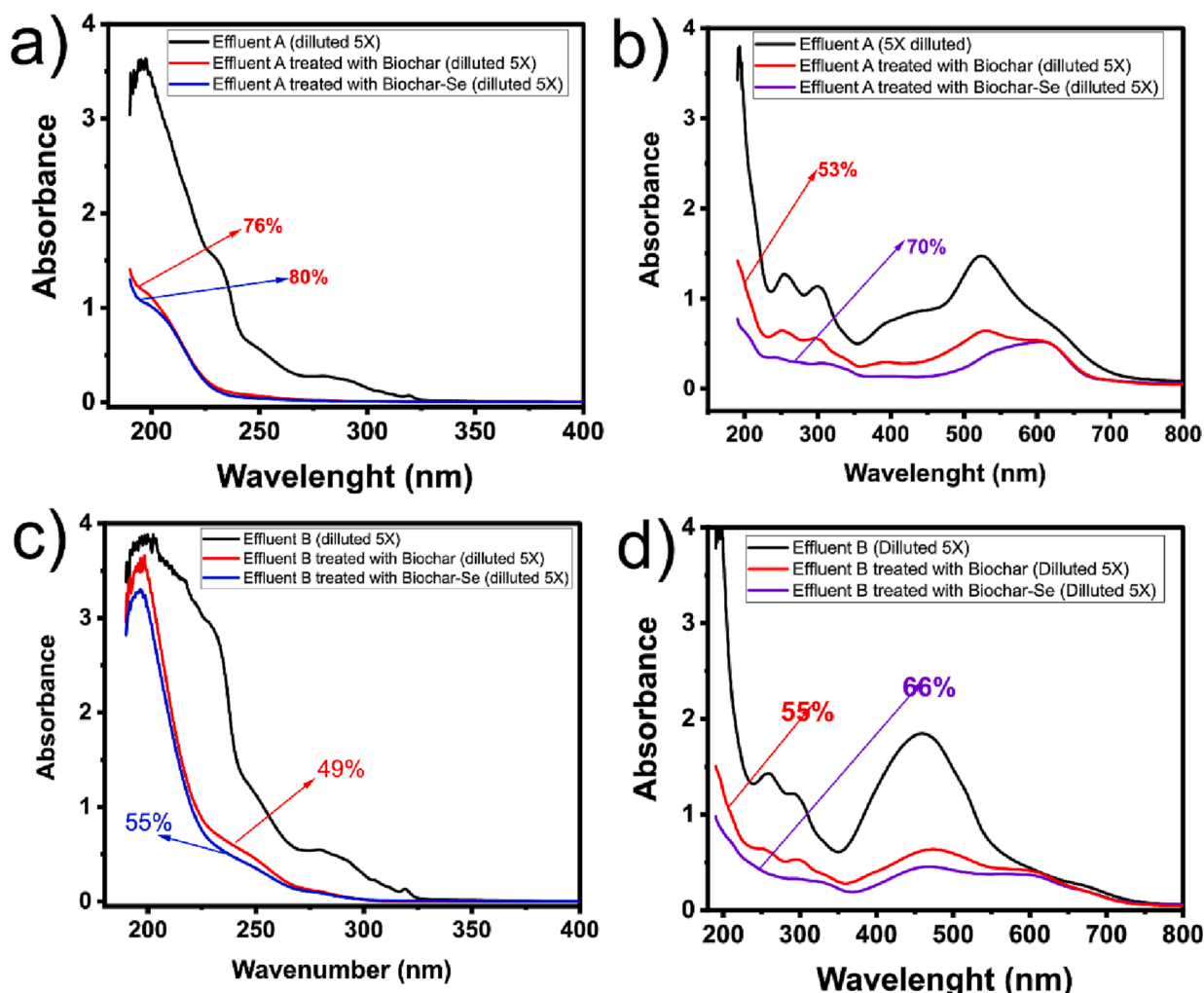
Fig. 10. Adsorption of synthetic effluents. a) Effluent A containing drugs; b) Effluent A containing dyes; c) Effluent B containing drugs, b) Effluent B containing dyes. See supplementary Table S1 and Supplementary Table S2 for compositions and types of the effluents. Conditions for the effluent adsorption: 298 K, adsorbent dosage of 1.0 g/L, and 250 rpm.

the treatment of real effluents. The UV–Vis spectra of the untreated and treated effluents with Biochar and Biochar-Se were recorded from 190 to 400 nm for the effluents containing drugs (see Fig. 10a,c), and from 190 to 800 nm for the effluents carried with dyes (see Fig. 10b,d). The areas under the absorption bands were used to calculate the percentage of the mixed compounds for the effluents.

The total of the compounds removal (in %) were 76% (Biochar) and 80% (Biochar-Se) for the effluent A (containing drugs), and 53% (Biochar) and 70% (Biochar-Se) for the effluent A (containing dyes). For the Effluents B, 49% (Biochar) and 55% (Biochar-Se) for the effluent-containing drugs (Fig. 10c), and 55% (Biochar) and 66% (Biochar-Se) for the effluent-containing dyes (Fig. 10d). These results evidence that despite Biochar-Se had better outcome in treating different effluents, pure biochar also presented good results, indicating their good suitability for treating effluents rich in organic–inorganic contaminants.

4. Conclusions

In the current study, biochar and biochar doped with Se were successfully synthesized by hydrothermal method followed by pyrolysis at 800 ^{0}C for 1 h. SEM-EDS, XPS, and XRD investigation revealed Se-doping in biochar. Biochar-Se acquired a rough surface and a less intact surface due to selenium doping, which exacerbated the physical defects on the doped biochar. The Biochar-Se sample was shown to have superior

adsorption capacity than the biochar sample for both DCF and RO-16 molecules. Acidic pH was found to be favorable for the adsorption of both DCF and RO-16. The maximum adsorption capacity of Se-Biochar was 355 mg g^{-1} for DCF and 538 mg g^{-1} for RO-16, according to data from the Liu isotherm model fitting. For both adsorbate molecules (DCF and RO-16) on Biochar and Biochar-Se adsorbents, the general order kinetic model showed the best fit for the experimental results. The key processes for both DCF and RO-16 adsorption on Biochar-Se were the formation of hydrogen bonds, π-π interactions, and electrostatic attraction. In Biochar-Se, the oxygen functionalities present on the surface of biochar can interact with Se-nanoparticles to form the metal–oxygen bond, resulting in physicochemical and electronic changes/defects on the adsorbent's surface which facilitate the metal–oxygen bond easier for binding DCF and RO-16 molecules. As a result, Se-biochar not only allows for the value-added use of waste biomass but it is also also effective in the removal of both dyes and drugs. Se-biochar can be considered a potential adsorbent material for water remediation.

Declaration of Competing Interest

Data availability

Data will be made available on request.

Acknowledgments

Appendix A. Supplementary data

Supplementary data to this article can be found online at https://doi.org/10.1016/j.ces.2023.119129.

References

Abadi, P.G., Irani, M., Rad, L.R., 2023. Mechanisms of the removal of the metal ions, dyes, and drugs from wastewaters by the electrospun nanofiber membranes. J. Taiwan Inst. Chem. Eng. 143, 104625 https://doi.org/10.1016/j.jtice.2022.104625.

Abdulhameed, A.S., Mohammad, A.-T., Jawad, A.H., 2019. Application of response surface methodology for enhanced synthesis of chitosan tripolyphosphate/TiO2 nanocomposite and adsorption of reactive orange 16 dye. J. Clean. Prod. 232, 43–56. https://doi.org/10.1016/j.jclepro.2019.05.291.

Ahmed, M.J., Danish, M., Anastopoulos, I., Iwuozor, K.O., 2023. Recent progress on corn (Zea mays L.)-based materials as raw, chemically modified, carbonaceous, and composite adsorbents for aquatic pollutants: A review. J. Anal. Appl. Pyrolysis 172, 106004. https://doi.org/10.1016/j.jaap.2023.106004.

Ajmal, A., Majeed, I., Malik, R.N., Idriss, H., Nadeem, M.A., 2014. Principles and mechanisms of photocatalytic dye degradation on TiO2 based photocatalysts: a comparative overview. RSC Adv. 4, 37003–37026. https://doi.org/10.1039/C4RA06658H.

Alfonso-Muniozguren, P., Serna-Galvis, E.A., Bussemaker, M., Torres-Palma, R.A., Lee, J., 2021. A review on pharmaceuticals removal from waters by single and combined biological, membrane filtration and ultrasound systems. Ultrason. Sonochem. 76, 105656 https://doi.org/10.1016/j.ultsonch.2021.105656.

Anastopoulos, I., Ahmed, M.J., Hummadi, E.H., 2022. Eucalyptus-based materials as adsorbents for heavy metals and dyes removal from (waste)waters. J. Mol. Liq. 356, 118864 https://doi.org/10.1016/j.molliq.2022.118864.

Anastopoulos, I., Giannopoulos, G., Islam, A., Ighalo, J.O., Iwuchukwu, F.U., Pashalidis, I., Kalderis, D., Giannakoudakis, D.A., Nair, V., Lima, E.C., 2022b. Chapter13 - Potential environmental applications of Helianthus annuus (sunflower) residue-based adsorbents for dye removal in (waste)waters, in: Anastopoulos, I., Lima, E., Meili, L., Giannakoudakis, D.B.T.-B.-D.M. for E.A. (Eds.), Elsevier, pp. 307–318. https://doi.org/https://doi.org/10.1016/B978-0-323-91914-2.00008-8.

Baccar, R., Sarrà, M., Bouzid, J., Feki, M., Blánquez, P., 2012. Removal of pharmaceutical compounds by activated carbon prepared from agricultural by-product. Chem. Eng. J. 211–212, 310–317. https://doi.org/10.1016/j.cej.2012.09.099.

Bagal, M.V., Gogate, P.R., 2014. Degradation of diclofenac sodium using combined processes based on hydrodynamic cavitation and heterogeneous photocatalysis. Ultrason. Sonochem. 21, 1035–1043. https://doi.org/10.1016/j.ultsonch.2013.10.020.

Bergmann, C., Machado, F., 2015. Carbon Nanomaterials as Adsorbents for Environmental and Biological Applications. Carbon. Nanostructures.

Bessa, V.S., Moreira, I.S., Tiritan, M.E., Castro, P.M.L., 2017. Enrichment of bacterial strains for the biodegradation of diclofenac and carbamazepine from activated sludge. Int. Biodeterior. Biodegrad. 120, 135–142. https://doi.org/10.1016/j.ibiod.2017.02.008.

Castañeda-Juárez, M., Martínez-Miranda, V., Almazán-Sánchez, P.T., Linares-Hernández, I., Santoyo-Tepole, F., Vázquez-Mejía, G., 2019. Synthesis of TiO2 catalysts doped with Cu, Fe, and Fe/Cu supported on clinoptilolite zeolite by an electrochemical-thermal method for the degradation of diclofenac by heterogeneous photocatalysis. J. Photochem. Photobiol. A Chem. 380, 111834 https://doi.org/10.1016/j.jphotochem.2019.04.045.

Cavalcante, E.H.M., Candido, I.C.M., de Oliveira, H.P., Silveira, K.B., de Souza, V., Álvares, T., Lima, E.C., Thyrel, M., Larsson, S.H., Simões dos Reis, G., 2022. 3-Aminopropyl-triethoxysilane-Functionalized Tannin-Rich Grape Biomass for the Adsorption of Methyl Orange Dye: Synthesis, Characterization, and the Adsorption Mechanism. ACS Omega 7, 18997–19009. https://doi.org/10.1021/acsomega.2c02101.

Cimirro, N.F.G.M., Lima, E.C., Cunha, M.R., Thue, P.S., Grimm, A., dos Reis, G.S., Rabiee, N., Saeb, M.R., Keivanimehr, F., Habibzadeh, S., 2022. Removal of diphenols using pine biochar. Kinetics, equilibrium, thermodynamics, and mechanism of uptake. J. Mol. Liq. 364, 119979 https://doi.org/10.1016/j.molliq.2022.119979.

de Azevedo, C.F., Machado, F.M., de Souza, N.F., Silveira, L.L., Lima, E.C., Andreazza, R., Bergamnn, C.P., 2023. Comprehensive adsorption and spectroscopic studies on the interaction of carbon nanotubes with diclofenac anti-inflammatory. Chem. Eng. J. 454, 140102 https://doi.org/10.1016/j.cej.2022.140102.

de Souza dos Santos, G.E., Ide, A.H., Duarte, J.L.S., McKay, G., Silva, A.O.S., Meili, L., 2020. Adsorption of anti-inflammatory drug diclofenac by MgAl/layered double hydroxide supported on Syagrus coronata biochar. Powder Technol. 364, 229–240.

Do Minh, T., Song, J., Deb, A., Cha, L., Srivastava, V., Sillanpää, M., 2020. Biochar based catalysts for the abatement of emerging pollutants: A review. Chem. Eng. J. 394, 124856.

dos Reis, G.S., Guy, M., Mathieu, M., Jebrane, M., Lima, E.C., Thyrel, M., Dotto, G.L., Larsson, S.H., 2022a. A comparative study of chemical treatment by MgCl2, ZnSO4, ZnCl2, and KOH on physicochemical properties and acetaminophen adsorption performance of biobased porous materials from tree bark residues. Colloids Surf. A Physicochem. Eng. Asp. 642, 128626 https://doi.org/10.1016/j.colsurfa.2022.128626.

dos Reis, G.S., Pinto, D., Lima, É.C., Knani, S., Grimm, A., Silva, L.F.O., Cadaval, T.R.S., Dotto, G.L., 2022b. Lanthanum uptake from water using chitosan with different configurations. React. Funct. Polym. 180, 105395 https://doi.org/10.1016/j.reactfunctpolym.2022.105395.

dos Reis, G.S., Bergna, D., Grimm, A., Lima, E.C., Hu, T., Naushad, M., Lassi, U., 2023a. Preparation of highly porous nitrogen-doped biochar derived from birch tree wastes with superior dye removal performance. Colloids Surf. A Physicochem. Eng. Asp. 669, 131493 https://doi.org/10.1016/j.colsurfa.2023.131493.

dos Reis, G.S., Larsson, S.H., Mathieu, M., Thyrel, M., Pham, T.N., 2023b. Application of design of experiments (DoE) for optimised production of micro- and mesoporous Norway spruce bark activated carbons. Biomass Conv. Bioref. 13 (11), 10113–10131.

Dotto, G.L., Vieillard, J., Pinto, D., Lütke, S.F., Silva, L.F.O., dos Reis, G.S., Lima, É.C., Franco, D.S.P., 2023. Selective adsorption of gadolinium from real leachate using a natural bentonite clay. J. Environ. Chem. Eng. 11, 109748 https://doi.org/10.1016/j.jece.2023.109748.

Feiqiang, G., Xiaolei, L., Xiaochen, J., Xingmin, Z., Chenglong, G., Zhonghao, R., 2018. Characteristics and toxic dye adsorption of magnetic activated carbon prepared from biomass waste by modified one-step synthesis. Colloids Surf. A Physicochem. Eng. Asp. 555, 43–54. https://doi.org/10.1016/j.colsurfa.2018.06.061.

Furlan, F.R., de Melo da Silva, L.G., Morgado, A.F., de Souza, A.A.U., Guelli Ulson de Souza, S.M.A., 2010. Removal of reactive dyes from aqueous solutions using combined coagulation/flocculation and adsorption on activated carbon. Resour. Conserv. Recycl. 54 (5), 283–290.

González-Hourcade, M., Simões dos Reis, G., Grimm, A., Dinh, V.M., Lima, E.C., Larsson, S.H., Gentili, F.G., 2022. Microalgae biomass as a sustainable precursor to produce nitrogen-doped biochar for efficient removal of emerging pollutants from aqueous media. J. Clean. Prod. 348, 131280 https://doi.org/10.1016/j.jclepro.2022.131280.

Guo, R., Yan, L., Rao, P., Wang, R., Guo, X., 2020. Nitrogen and sulfur co-doped biochar derived from peanut shell with enhanced adsorption capacity for diethyl phthalate. Environ. Pollut. 258, 113674 https://doi.org/10.1016/j.envpol.2019.113674.

He, L., Qiu, Y., Yao, C., Lan, G., Li, N., Zhou, H., Liu, Q., Sun, X., Cheng, Z., Li, Y., 2023. Role of intrinsic defects on carbon adsorbent for enhanced removal of Hg2+ in aqueous solution. Chinese J. Chem. Eng. https://doi.org/https://doi.org/10.1016/j.cjche.2023.03.021.

Jansen, S., Konrad, H., Geburek, T., 2017. The extent of historic translocation of Norway spruce forest reproductive material in Europe. Ann. For. Sci. 74, 56. https://doi.org/10.1007/s13595-017-0644-z.

Jin, Z., Nie, H., Yang, Z., Zhang, J., Liu, Z., Xu, X., Huang, S., 2012. Metal-free selenium doped carbon nanotube/graphene networks as a synergistically improved cathode catalyst for oxygen reduction reaction. Nanoscale 4, 6455–6460. https://doi.org/10.1039/C2NR31858J.

Jodeh, S., Abdelwahab, F., Jaradat, N., Warad, I., Jodeh, W., 2016. Adsorption of diclofenac from aqueous solution using Cyclamen persicum tubers based activated carbon (CTAC). J. Assoc. Arab Univ. Basic Appl. Sci. 20, 32–38. https://doi.org/10.1016/j.jaubas.2014.11.002.

Kalderis, D., Seifi, A., Kieu Trang, T., Tsubota, T., Anastopoulos, I., Manariotis, I., Pashalidis, I., Khataee, A., 2023. Bamboo-derived adsorbents for environmental remediation: A review of recent progress. Environ. Res. 224, 115533 https://doi.org/10.1016/j.envres.2023.115533.

Kazeem, T.S., Lateef, S.A., Ganiyu, S.A., Qamaruddin, M., Tanimu, A., Sulaiman, K.O., Sajid Jillani, S.M., Alhooshani, K., 2018. Aluminium-modified activated carbon as efficient adsorbent for cleaning of cationic dye in wastewater. J. Clean. Prod. 205, 303–312. https://doi.org/10.1016/j.jclepro.2018.09.114.

Kheradmand, A., Negarestani, M., Kazemi, S., Shayesteh, H., Javanshir, S., Ghiasinejad, H., 2022. Adsorption behavior of rhamnolipid modified magnetic Co/Al layered double hydroxide for the removal of cationic and anionic dyes. Sci. Rep. 12, 14623. https://doi.org/10.1038/s41598-022-19056-0.

la Farré, M., Pérez, S., Kantiani, L., Barceló, D., 2008. Fate and toxicity of emerging pollutants, their metabolites and transformation products in the aquatic environment. TrAC Trends Anal. Chem. 27, 991–1007. https://doi.org/10.1016/j.trac.2008.09.010.

Liang, C., Wei, D., Zhang, S., Ren, Q., Shi, J., Liu, L., 2021. Removal of antibiotic resistance genes from swine wastewater by membrane filtration treatment.

Ecotoxicol. Environ. Saf. 210, 111885 https://doi.org/10.1016/j.ecoenv.2020.111885.

Lima, É.C., Adebayo, M.A., Machado, F.M., 2015. In: Kinetic and Equilibrium Models of Adsorption BT - Carbon Nanomaterials as Adsorbents for Environmental and Biological Applications. Springer International Publishing, Cham, pp. 33–69. https://doi.org/10.1007/978-3-319-18875-1_3.

Lima, F.S., de, E.L., Barros Neto, Melo, R.P.F., da, J.M., Silva, Neto, Bezerra, F.W., Lopes, de, Jesus, Nogueira, Duarte,, L.,, 2022. Removal of diclofenac sodium from aqueous solution using ionic micellar flocculation-assisted adsorption. Sep. Sci. Technol. 57, 2997–3011. https://doi.org/10.1080/01496395.2022.2085577.

Lin, L., Yang, H., Xu, X., 2022. Effects of Water Pollution on Human Health and Disease Heterogeneity: A Review. Front. Environ. Sci. 10 https://doi.org/10.3389/fenvs.2022.880246.

Liu, J., Bahadoran, A., Emami, N., Al-Musawi, T.J., Dawood, F.A., Nasajpour-Esfahani, N., Najafipour, I., Mousavi, S.E., Ghazuan, T., Mosallanezhad, M., Toghraie, D., 2023. Removal of diclofenac sodium and cefixime from wastewater by polymeric PES mixed-matrix-membranes embedded with MIL101-OH/Chitosan. Process Saf. Environ. Prot. 172, 588–593. https://doi.org/10.1016/j.psep.2023.02.060.

Liu, Y., Dai, H., An, Y., Fu, L., An, Q., Wu, Y., 2020. Facile and scalable synthesis of a sulfur{,} selenium and nitrogen co-doped hard carbon anode for high performance Na- and K-ion batteries. J. Mater. Chem. A 8, 14993–15001. https://doi.org/10.1039/D0TA04513F.

Luo, C., Wang, J., Suo, L., Mao, J., Fan, X., Wang, C., 2015. In situ formed carbon bonded and encapsulated selenium composites for Li–Se and Na–Se batteries. J. Mater. Chem. A 3, 555–561. https://doi.org/10.1039/C4TA04611K.

Malakootian, M., Heidari, M.R., 2018. Reactive orange 16 dye adsorption from aqueous solutions by psyllium seed powder as a low-cost biosorbent: kinetic and equilibrium studies. Appl. Water Sci. 8, 212. https://doi.org/10.1007/s13201-018-0851-2.

Malek, N.N.A., Jawad, A.H., Ismail, K., Razuan, R., ALOthman,, Z.A.,, 2021. Fly ash modified magnetic chitosan-polyvinyl alcohol blend for reactive orange 16 dye removal: Adsorption parametric optimization. Int. J. Biol. Macromol. 189, 464–476. https://doi.org/10.1016/j.ijbiomac.2021.08.160.

Moreira, I.S., Bessa, V.S., Murgolo, S., Piccirillo, C., Mascolo, G., Castro, P.M.L., 2018. Biodegradation of Diclofenac by the bacterial strain Labrys portucalensis F11. Ecotoxicol. Environ. Saf. 152, 104–113. https://doi.org/10.1016/j.ecoenv.2018.01.040.

Muralikrishnan, R., Jodhi, C., 2021. Biodecolorization of Reactive Orange 16 using biochar produced from groundnut shell (Arachis hypogaea): batch, isotherm, kinetic, and regeneration studies. Biomass Conv. Bioref. 13 (10), 8891–8902.

Naddeo, V., Belgiorno, V., Kassinos, D., Mantzavinos, D., Meric, S., 2010. Ultrasonic degradation, mineralization and detoxification of diclofenac in water: Optimization of operating parameters. Ultrason. Sonochem. 17, 179–185. https://doi.org/10.1016/j.ultsonch.2009.04.003.

Nizam, N.U.M., Hanafiah, M.M., Mahmoudi, E., Halim, A.A., Mohammad, A.W., 2021. The removal of anionic and cationic dyes from an aqueous solution using biomass-based activated carbon. Sci. Rep. 11, 8623. https://doi.org/10.1038/s41598-021-88084-z.

Omorogie, M.O., Babalola, J.O., Ismaeel, M.O., McGettrick, J.D., Watson, T.M., Dawson, D.M., Carta, M., Kuehnel, M.F., 2021. Activated carbon from Nauclea diderrichii agricultural waste–a promising adsorbent for ibuprofen, methylene blue and CO2. Adv. Powder Technol. 32, 866–874. https://doi.org/10.1016/j.apt.2021.01.031.

Ong, C., Lee, K., Chang, Y., 2020. Biodegradation of mono azo dye-Reactive Orange 16 by acclimatizing biomass systems under an integrated anoxic-aerobic REACT sequencing batch moving bed biofilm reactor. J. Water Process Eng. 36, 101268 https://doi.org/10.1016/j.jwpe.2020.101268.

Pawlyta, M., Rouzaud, J.-N., Duber, S., 2015. Raman microspectroscopy characterization of carbon blacks: Spectral analysis and structural information. Carbon N. Y. 84, 479–490. https://doi.org/10.1016/j.carbon.2014.12.030.

Piergrossi, V., Fasolato, C., Capitani, F., Monteleone, G., Postorino, P., Gislon, P., 2019. Application of Raman spectroscopy in chemical investigation of impregnated activated carbon spent in hydrogen sulfide removal process. Int. J. Environ. Sci. Technol. 16, 1227–1238. https://doi.org/10.1007/s13762-018-1756-1.

Piri, M., Heravi, M.M., Elhampour, A., Nemati, F., 2021. Silver nanoparticles supported on P, Se-codoped g-C3N4 nanosheet as a novel heterogeneous catalyst for reduction of nitroaromatics to their corresponding amines. J. Mol. Struct. 1242, 130646 https://doi.org/10.1016/j.molstruc.2021.130646.

Pramono, E., Umam, K., Sagita, F., Saputra, O.A., Alfiansyah, R., Setyawati Dewi, R.S., Kadja, G.T.M., Ledyastuti, M., Wahyuningrum, D., Radiman, C.L., 2023. The enhancement of dye filtration performance and antifouling properties in amino-functionalized bentonite/polyvinylidene fluoride mixed matrix membranes. Heliyon 9. https://doi.org/10.1016/j.heliyon.2023.e12823.

Qian, H., Hou, Q., Yu, G., Nie, Y., Bai, C., Bai, X., Ju, M., 2020. Enhanced removal of dye from wastewater by Fenton process activated by core-shell NiCo2O4@FePc catalyst. J. Clean. Prod. 273, 123028 https://doi.org/10.1016/j.jclepro.2020.123028.

Rafiq, A., Ikram, M., Ali, S., Niaz, F., Khan, M., Khan, Q., Maqbool, M., 2021. Photocatalytic degradation of dyes using semiconductor photocatalysts to clean

industrial water pollution. J. Ind. Eng. Chem. 97, 111–128. https://doi.org/10.1016/j.jiec.2021.02.017.

Ravindiran, G., Gaddam, K., Sunil, K., Chelladurai, S.J.S., 2022. Experimental Investigation on Reactive Orange 16 Removal Using Waste Biomass of Ulva prolifera. Adv. Mater. Sci. Eng. 2022, 1–8.

Rostamian, R., Behnejad, H., 2018. A comprehensive adsorption study and modeling of antibiotics as a pharmaceutical waste by graphene oxide nanosheets. Ecotoxicol. Environ. Saf. 147, 117–123. https://doi.org/10.1016/j.ecoenv.2017.08.019.

Shah, J.A., Butt, T.A., Mirza, C.R., Shaikh, A.J., Khan, M.S., Arshad, M., Riaz, N., Haroon, H., Gardazi, S.M.H., Yaqoob, K., Bilal, M., 2020. Phosphoric Acid Activated Carbon from Melia azedarach Waste Sawdust for Adsorptive Removal of Reactive Orange 16: Equilibrium Modelling and Thermodynamic Analysis. Molecules 25 (9), 2118.

Shirani, Z., Song, H., Bhatnagar, A., 2020. Efficient removal of diclofenac and cephalexin from aqueous solution using Anthriscus sylvestris-derived activated biochar. Sci. Total Environ. 745, 140789 https://doi.org/10.1016/j.scitotenv.2020.140789.

Simović, B., Radovanović, Ž., Branković, G., Dapčević, A., 2023. Hydrothermally synthesized CeO2/ZnO nanocomposite photocatalysts for the enhanced degradation of Reactive Orange 16 dye. Mater. Sci. Semicond. Process. 162, 107542 https://doi.org/10.1016/j.mssp.2023.107542.

Thakur, V., Sharma, P., Awasthi, A., Guleria, A., Singh, K., 2023. Utility of acrylic acid grafted lignocellulosic waste sugarcane bagasse for the comparative study of cationic and anionic dyes adsorption applications. Environ. Nanotechnol. Monit. Manag. 20, 100824 https://doi.org/10.1016/j.enmm.2023.100824.

Thommes, M., Kaneko, K., Neimark, A.V., Olivier, J.P., Rodriguez-Reinoso, F., Rouquerol, J., Sing, K.S.W., 2015. Physisorption of gases, with special reference to the evaluation of surface area and pore size distribution. Pure Appl. Chem. 87, 1051–1069. https://doi.org/10.1515/pac-2014-1117.

Usman, M., Anastopoulos, I., Hamid, Y., Wakeel, A., 2022. Recent trends in the use of fly ash for the adsorption of pollutants in contaminated wastewater and soils: Effects on soil quality and plant growth. Environ. Sci. Pollut. Res. https://doi.org/10.1007/s11356-022-19192-0.

Wang, X., Li, F., Hu, X., Hua, T., 2021. Electrochemical advanced oxidation processes coupled with membrane filtration for degrading antibiotic residues: A review on its potential applications, advances, and challenges. Sci. Total Environ. 784, 146912 https://doi.org/10.1016/j.scitotenv.2021.146912.

Wang, T., Xue, L., Liu, Y., Fang, T., Zhang, L., Xing, B., 2022. Insight into the significant contribution of intrinsic defects of carbon-based materials for the efficient removal of tetracycline antibiotics. Chem. Eng. J. 435, 134822 https://doi.org/10.1016/j.cej.2022.134822.

Weidner, E., Karbassiyazdi, E., Altaee, A., Jesionowski, T., Ciesielczyk, F., 2022. Hybrid Metal Oxide/Biochar Materials for Wastewater Treatment Technology: A Review. ACS Omega 7, 27062–27078. https://doi.org/10.1021/acsomega.2c02909.

Xie, J., Liu, M., He, M., Liu, Y., Li, J., Yu, F., Lv, Y., Lin, C., Ye, X., 2023. Ultra-efficient adsorption of diclofenac sodium on fish-scale biochar functionalized with H3PO4 via synergistic mechanisms. Environ. Pollut. 322, 121226 https://doi.org/10.1016/j.envpol.2023.121226.

Xu, D., Li, Z., Wang, P., Bai, W., Wang, H., 2020. Aquatic plant-derived biochars produced in different pyrolytic conditions: Spectroscopic studies and adsorption behavior of diclofenac sodium in water media. Sustain. Chem. Pharm. 17, 100275 https://doi.org/10.1016/j.scp.2020.100275.

Yang, X., Wan, Y., Zheng, Y., He, F., Yu, Z., Huang, J., Wang, H., Ok, Y.S., Jiang, Y., Gao, B., 2019. Surface functional groups of carbon-based adsorbents and their roles in the removal of heavy metals from aqueous solutions: A critical review. Chem. Eng. J. 366, 608–621. https://doi.org/10.1016/j.cej.2019.02.119.

Yu, C.-X., Chen, J., Zhang, Y., Song, W.-B., Li, X.-Q., Chen, F.-J., Zhang, Y.-J., Liu, D., Liu, L.-L., 2021. Highly efficient and selective removal of anionic dyes from aqueous solution by using a protonated metal-organic framework. J. Alloys Compd. 853, 157383 https://doi.org/10.1016/j.jallcom.2020.157383.

Zhang, M., Dong, H., Zhao, L., Wang, D., Meng, D., 2019. A review on Fenton process for organic wastewater treatment based on optimization perspective. Sci. Total Environ. 670, 110–121. https://doi.org/10.1016/j.scitotenv.2019.03.180.

Zhang, B., Zhang, J., Zhang, F., Zheng, L., Mo, G., Han, B., Yang, G., 2020a. Selenium-Doped Hierarchically Porous Carbon Nanosheets as an Efficient Metal-Free Electrocatalyst for CO2 Reduction. Adv. Funct. Mater. 30, 1906194. https://doi.org/10.1002/adfm.201906194.

Zhang, B., Mei, M., Li, K., Liu, J., Wang, T., Chen, S., Li, J., 2022. One-pot synthesis of MnFe2O4 functionalized magnetic biochar by the sol-gel pyrolysis method for diclofenac sodium removal. J. Clean. Prod. 381, 135210 https://doi.org/10.1016/j.jclepro.2022.135210.

Zhang, H., Tu, Y.-J., Duan, Y.-P., Liu, J., Zhi, W., Tang, Y., Xiao, L.-S., Meng, L., 2020b. Production of biochar from waste sludge/leaf for fast and efficient removal of diclofenac. J. Mol. Liq. 299, 112193 https://doi.org/10.1016/j.molliq.2019.112193.

Žur, J., Piński, A., Marchlewicz, A., Hupert-Kocurek, K., Wojcieszyńska, D., Guzik, U., 2018. Organic micropollutants paracetamol and ibuprofen—toxicity, biodegradation, and genetic background of their utilization by bacteria. Environ. Sci. Pollut. Res. 25, 21498–21524. https://doi.org/10.1007/s11356-018-2517-x.